

# Off-center deflagrations in Chandrasekhar mass SN Ia models

J.C. Niemeyer, W. Hillebrandt, and S.E. Woosley<sup>1</sup>

*Max Planck Institut für Astrophysik, Karl Schwarzschild Str.1, 85740 Garching, Germany*

## ABSTRACT

A series of two dimensional numerical simulations of explosive nuclear burning is presented for white dwarfs near the Chandrasekhar mass. We assume that the burning begins as a slow deflagration front at or near the center of the star, and continues until the density in the burning regions has declined to about  $10^7 \text{ g cm}^{-3}$ , where the flame is essentially extinguished. We employ a novel numerical representation of the turbulent flame brush based upon ideas previously developed for modelling laboratory combustion and explore in some detail the sensitivity of the outcome to the manner in which burning is initiated. In particular, we simulate 1) a centrally ignited deflagration, 2) off-center ignition at a single “point”, and 3) simultaneous off-center ignition at five “points”. We find that the amount of  $^{56}\text{Ni}$  that is produced and other observable properties depend sensitively upon how the fuel is ignited. Because of the immediate onset of buoyant acceleration, the burning region in models ignited off center rises toward the surface more quickly than in the (commonly assumed) case of central ignition. With the exception of the model that ignited off-center at a single point, all models are unbound at the end of the computations and between  $0.59 M_{\odot}$  (central ignition) and  $0.65 M_{\odot}$  (ignition at multiple “points”) of matter are processed into nuclear burning products. These results would guarantee an observable, though weak, Type Ia supernova. Our results are expected to change for simulations in three dimensions, especially for the off-center ignitions discussed in this paper, and late detonations driven by pulsations are not unambiguously excluded. We can, however, state that the chances for a direct transition to a detonation appear small because, in all our models, the turbulent velocity of the burning front remains very subsonic.

---

<sup>1</sup>permanent address: Board of Studies in Astronomy and Astrophysics, University of California, Santa Cruz, CA 95064

## 1. Introduction

The mechanism whereby an accreting carbon-oxygen white dwarf explodes as a Type Ia supernova continues to be uncertain. While considerable recent attention has been given to the so called “sub-Chandrasekhar mass models” (e.g., Iben & Tutukov 1991, Limongi & Tornambe 1991, Kenyon *et al.* 1993, Munari & Renzini 1992, Woosley & Weaver 1994, Livne & Arnett 1996), there remain compelling reasons to think that a portion, perhaps most Type Ia supernovae are the explosion of dwarfs that have approached the Chandrasekhar mass,  $M_{\text{chan}} \approx 1.39 M_{\odot}$ . These reasons include: 1) the recent identification of supersoft x-ray sources (Rappaport, DiStefano, & Smith 1994) as the possible progenitors; 2) the requirement of conditions that exist only in this class of model for the nucleosynthesis of the isotopes  $^{48}\text{Ca}$ ,  $^{54}\text{Cr}$ , and  $^{50}\text{Ti}$  (Woosley & Weaver 1986, Woosley & Eastman 1995); 3) the good agreement of the prototypical  $M_{\text{chan}}$  model, W7 (Nomoto, Thielemann & Yokoi 1984) with the observed spectra of typical Type Ia supernovae; 4) the good agreement with light curves from this class of model with a variety of Type Ia supernovae (Höflich & Khokhlov 1996); and 5) the difficulty achieving a robust explosion in three dimensional sub- $M_{\text{chan}}$  models (Benz 1996, Garcia-Senz, Bravo, & Woosley 1996).

Despite this evidence, there remains great uncertainty both as to whether growth of the CO dwarf to  $M_{\text{chan}}$  is frequently realized and the nature of the nuclear explosion once it has begun (Niemeyer & Woosley 1996). The similarity of the progenitor star mass, and therefore of the initial density structure, suggests a common outcome from this kind of event. However, there are properties of the progenitor star - the accretion rate, the original mass of the CO white dwarf before accretion began, its carbon to oxygen ratio, the metallicity, and perhaps its rotation rate - that might lead to diversity. Garcia-Senz & Woosley 1995 (GW), in particular, have suggested that small initial differences might be amplified because the convective runaway that precedes the explosion may lead to ignition at multiple and unpredictable locations. If the global characteristics of the event, i.e. the ejecta composition and energy, depended strongly on the ignition conditions some spread of outcomes would follow as a natural consequence.

Previous multi-dimensional simulations of  $M_{\text{chan}}$  explosions have studied the dynamics of *centrally* ig-

nited flame fronts with perturbed surfaces that first go through the linear Raleigh-Taylor (RT) instability phase, and later develop rising bubbles of hot, burned material and turbulence (Müller & Arnett 1986, Livne 1993, Khokhlov 1995, Niemeyer & Hillebrandt 1995). This assumption of central ignition simplifies the calculation and seemed reasonable based upon existing one dimensional models of the pre-explosive evolution. Unfortunately, these models all share a common fate - an inadequate amount of burning occurs to produce a credible explosion. This has led some to speculate (Khokhlov 1995, Arnett & Livne 1994a, Arnett & Livne 1994b, Niemeyer & Woosley 1996) that the explosion must follow one or more pulsations of the white dwarf in which energy is shared between ashes and fuel and a detonation occurs.

Here, we take a different approach, returning to the simple (non-pulsing) deflagration models and considering the effects of off center and multiple point ignition. While our immediate motivation is the work of GW, there are other lines of reasoning (e.g., Iben 1982) that also suggest off-center ignition. In the GW model ignition points are set by conditions inside the star when its central temperature reaches  $6 \times 10^8$  K. At this point the time for nuclear burning and the convective cycle of a burning bubble become comparable. For certain circumstances, which the star may naturally realize as it continuously increases its burning rate, rising bubbles of carbon continue to burn and become more buoyant as they float in an evolution that is distinctly non-adiabatic. GW’s model suggests that the flame is born on the surfaces of rising buoyant bubbles with a typical diameter of about 10 km, at a radial distance between 100 and 200 km off-center.

To follow these rising burning bubbles, we employ a novel prescription for flame tracking. Usually the macroscopic burning front is numerically represented by a thin interface that propagates into the unburned fuel with a prescribed speed (Livne 1993, Khokhlov 1993, Khokhlov 1994, Khokhlov 1995, Niemeyer & Hillebrandt 1995). Here we use a “turbulent flame brush” whose properties are discussed in section (2). Because the prescription is new we calculated both centrally and non-centrally ignited flames for comparison.

We find that the amount of  $^{56}\text{Ni}$  that is produced, the overall energy released, and especially the radial distribution of the burning products are all quite sensitive to how ignition is simulated. However, we

are unable to conclude unambiguously from the two-dimensional studies whether the star explodes on the first try or pulses. Continued studies in three dimensions that calculate the evolution for a longer time as well as a better understanding of turbulent flame physics will be necessary to resolve this point.

## 2. Numerical representation of the turbulent flame brush

Owing to the enormous difference between the grid resolution of multidimensional SN Ia simulations,  $\Delta \approx 10$  km, and the thickness of laminar thermonuclear flames,  $l_{\text{th}} \approx 10^{-4}$  cm, it is impossible to use the nuclear rate equations, evaluated at the grid averaged temperature  $\bar{T}_\Delta$  and density  $\bar{\rho}_\Delta$ , to directly compute the energy generation rate  $\dot{S}$  of a zone that contains fragments of the turbulent flame brush (“flamelets”) (Livne 1993, Khokhlov 1993, Arnett & Livne 1994b, Khokhlov 1995, Niemeyer & Hillebrandt 1995). In other words, one has to suitably transform the strongly peaked, unresolved reaction structure of flamelets immersed in unburned fuel into an average value for  $\dot{S}$  of the whole zone. Furthermore, the propagation speed and thickness of the burning front have to be modeled in a realistic fashion. Previously, all this has been done by decoupling the numerical flame front from the grid averaged thermodynamic quantities and using an artificial scheme to propagate a thin interface separating fuel and ashes with a prescribed “turbulent” flame speed  $u(\Delta)$ . The latter can be obtained by invoking isotropic turbulence, in which case a thick “turbulent flame brush” develops that propagates roughly at the speed of the largest unresolved eddies  $v(\Delta)$  (Niemeyer & Hillebrandt 1995, Niemeyer & Woosley 1996).

However, total decoupling from the thermodynamic state of the numerical cell prevents fluid expansion or compression from directly affecting the flame. Only by introducing further artificial rules can local ignition or quenching of the flame by temperature changes be included in these schemes. An alternative way to treat the problem is to couple the grid temperature  $\bar{T}_\Delta$  to the energy generation rate via the burning time  $\tau_{\text{burn}} = \epsilon_{\text{nuc}}/\dot{S}$ . Obviously, if the physical burning times were known in each zone, the code would be able to decide whether to assume the presence of highly localized flamelets in the zone, or else to burn slowly and homogeneously as it does prior to flame ignition. We therefore state the main assumption

of our flame model:

$$\bar{\tau}_{\text{burn}\Delta}(\rho, T, X_{i\Delta}) \approx \tau_{\text{burn}}(\bar{\rho}_\Delta, \bar{T}_\Delta, \bar{X}_{i\Delta}). \quad (1)$$

This assumption is reasonably well satisfied. Immediately after the flame front enters a grid zone, nuclear energy is deposited into the zone in the form of internal energy  $\bar{\epsilon}_{i\Delta}$ . By virtue of the small heat capacity  $c_p$  of degenerate matter, reflected by the numerical equation of state, and the relation  $dT \sim c_p^{-1} d\epsilon_i$ , small growth of  $\bar{\epsilon}_{i\Delta}$  already leads to a strong rise of the zone temperature  $\bar{T}_\Delta$ . Consequently,  $\bar{T}_\Delta$  quickly approaches the final temperature  $T_b$  of the burned mixture, even if only a small part of the zone is burned. The *numerical* burning time as computed from the grid averaged temperature (the *rhs* of equation 1) is thus mostly evaluated at  $\bar{T}_\Delta \approx T_b$ . This is consistent with the fact that the *physical*, grid averaged burning time (the *lhs* of equation 1) is also dominated by burning at  $T_b$  due to the strong temperature dependence of  $\dot{S}$ .

In order to distinguish between low temperature, volume filling burning that is fully resolved by the grid and the high temperature regime that gives rise to flame formation,  $\tau_{\text{burn}}$  must be related to the characteristic length scale of burning regions. To this end, we invoke the stationarity assumption  $\tau_{\text{burn}} = \tau_{\text{trans}}$ , where  $\tau_{\text{trans}}$  stands for the heat transport time scale (Landau & Lifshitz 1991). Two different transport mechanisms compete on all scales: thermal conduction and turbulent transport. Both can be described by transport coefficients that connect  $\tau_{\text{trans}}$  (and, hence,  $\tau_{\text{burn}}$ ) to the burning length  $l_{\text{burn}}$  via

$$\tau_{\text{cond}} = \frac{\rho c_p l_{\text{burn}}^2}{\sigma}, \quad \tau_{\text{tur}} = \frac{l_{\text{burn}}^2}{\nu_{\text{tur}}}. \quad (2)$$

The turbulent transport coefficient is the so-called “eddy viscosity”  $\nu_{\text{tur}} \propto v(\Delta) \Delta$ , where  $v(\Delta)$  again denotes the mean magnitude of turbulent velocity fluctuations on the grid scale. One possible technique to compute  $v(\Delta)$  and  $\nu_{\text{tur}}$  with the help of a subgrid (SG) model for the unresolved turbulent kinetic energy  $q \approx v(\Delta)^2/2$  was employed by Niemeyer & Hillebrandt 1995 for SN Ia calculations; the same method was applied in this work. One must be cautious, however, to evaluate the eddy viscosity at the burning length scale, that is

$$\begin{aligned} \nu_{\text{tur}} &= \nu_{\text{tur}}(l_{\text{burn}}) \\ &= \nu_{\text{tur}}(\Delta) \left( \frac{l_{\text{burn}}}{\Delta} \right)^{4/3}, \end{aligned} \quad (3)$$

where we have used the Kolmogorov scaling law  $v(l) \propto l^{1/3}$ . Turbulent transport is realized on larger scales while at the same time, thermal conduction dominates small scale diffusion owing to the different scaling behaviour of both transport coefficients. Whereas  $\nu_{\text{tur}}$  depends on turbulent velocity fluctuations that decay on small scales, thermal conduction by electrons takes over on microscopic scales. The position of this transition is defined by the burning time (and, therefore, by temperature). Equations (3) and (2) yield the burning lengths at given  $\tau_{\text{burn}}$  corresponding to both transport mechanisms:

$$l_{\text{cond}} = \sqrt{\frac{\tau_{\text{burn}} \sigma}{c_p \rho}} \quad , \quad l_{\text{tur}} = (\tau_{\text{burn}} \nu_{\text{tur}}(\Delta))^{3/2} \Delta^{-2} . \quad (4)$$

Fig. (1) demonstrates the behaviour of both quantities at a typical turbulent intensity and density for thermonuclear flames in white dwarfs. Since the microscopic burning time at  $T_b \approx 8 \times 10^9$  K in the flamelet regime is  $\tau_{\text{burn}} \approx 10^{-12}$  s, the graph shows that microscopic flame dynamics are governed by thermal conduction.

Phenomenologically, the burning regime that is realized at a given temperature is the one with the maximum burning length:

$$l_{\text{burn}} = \max(l_{\text{cond}}, l_{\text{tur}}) . \quad (5)$$

If  $l_{\text{burn}} \gtrsim \Delta$ , the burning region is fully resolved and the energy generation rate is given directly by the nuclear reaction rate. This only occurs prior to ignition of the zone by the spreading flame brush. In case of  $l_{\text{burn}} < \Delta$ , the energy generation rate can only be computed by means of the effective flame speed  $u(\Delta)$ , for reasons explained above. Two further sub-cases are possible: if  $l_{\text{burn}} = l_{\text{tur}}$ , the zone is not yet hot enough to burn in the flamelet regime, as turbulent transport still dominates at the burning scale. We can approximate the effective ‘‘flame speed’’ in this transition regime (corresponding to the preheating region of laminar flames) by  $u(\Delta) \approx l_{\text{burn}}/\tau_{\text{burn}}$ . As soon as the flame brush fully enters the zone, the temperature rises to the point where flame transport is governed by thermal conduction on the scales defined by the burning time, i.e.,  $l_{\text{burn}} = l_{\text{cond}} \ll \Delta$ . The effective *macroscopic* burning speed then follows from the maximum of all competing transport velocities at the grid scale:

$$u(\Delta) = \max(u_{\text{lam}}, v(\Delta), v_{\text{rt}}(\Delta)) , \quad (6)$$

where  $u_{\text{lam}}$  represents the laminar flame speed, adopted from Timmes & Woosley 1992. Here,  $v_{\text{rt}}(\Delta)$  is the asymptotic velocity of rising buoyant bubbles with the radius  $\Delta$ :

$$v_{\text{rt}}(\Delta) = \mathcal{B} \sqrt{g_{\text{eff}} \Delta} \quad (7)$$

(Layzer 1955), where  $\mathcal{B} = 0.511$  is a constant,  $g_{\text{eff}} = Atg$  is the effective gravitational acceleration, and the Atwood number  $At = (\rho_u - \rho_b)/(\rho_u + \rho_b)$  is a measure for the density contrast of burned (b) and unburned (u) material. Khokhlov 1995 confirmed that RT-unstable flames in tubes with the radius  $\Delta$  propagate with a speed given by equation (7) with the help of three-dimensional simulations. In our calculations, however, we used a smaller coefficient ( $\mathcal{B} = 0.25$ ) than the single-bubble value derived by Layzer in order to account for the presence of many bubbles with smaller radii in one cell. The turbulent fluctuation velocity  $v(\Delta)$  is obtained directly from the kinetic SG-energy:

$$v(\Delta) = \sqrt{2q} . \quad (8)$$

The effective energy generation rate is then calculated from

$$\overline{(\rho \dot{S})}_{\Delta} \equiv \frac{1}{\Delta^3} \int_{V_{\Delta}} d^3x \rho \dot{S} \approx \frac{u(\Delta) \bar{\rho}_{\Delta} \epsilon_{\text{nuc}}}{\Delta} . \quad (9)$$

Assumption (1) enables us to determine the presence of flame segments in a given zone. Therefore, no artificial prescription for the thickness of the flame brush is required, since its structure is now fully determined by the temperature and fuel mass fraction of the fluid. Moreover, the flame is now allowed to spontaneously ignite if the temperature increases sufficiently (e.g., by compression) to yield a burning time that indicates the formation of localized energy sources.

In addition to the energy generation rate the model has to provide proper propagation of the flame surface. A possible method follows in a very natural way from the fact that temperature is used as an indicator of flame presence. The diffusion of internal energy by unresolved turbulent motions is equivalent to thermal conduction with a modified transport coefficient which is of the same order of magnitude as the eddy viscosity. Since the eddy viscosity is known from the SG-model, turbulent energy diffusion can be parameterized by

$$\begin{aligned} \mathbf{h} &= \rho C_{\epsilon_1} \nu_{\text{tur}} \nabla \epsilon_1 \\ &= \rho C_{\epsilon_1} \nu_{\text{tur}} c_p \nabla \bar{T} \end{aligned} \quad (10)$$

if the specific heat  $c_p$  is assumed to be locally constant. The constant  $C_{\epsilon_i}$  is of order unity; it has been calibrated by numerical tests to provide the correct flame speed (see Niemeyer 1995 for details). Equation (10) shows that a temperature jump spreads over the distance  $\Delta$  by turbulent diffusion during a characteristic time  $\tau_{\text{diff}} \approx \Delta^2/\nu_{\text{tur}} \approx \Delta/v(\Delta)$ . Since the burning timescale of a turbulent flame on the scale  $\Delta$  that moves at a speed of  $u(\Delta) \approx v(\Delta)$  is equally given by  $\Delta/v(\Delta)$  we see that the proposed flame model is self-consistent in the turbulent burning regime: the boundary of the high temperature region moves with the speed of a turbulent flame front.

### 3. Simulations of central and off-center ignitions

The simulations involved an Eulerian PPM-based code to solve the two-dimensional hydrodynamical equations. Specifically, we employed the program PROMETHEUS (Fryxell *et al.* 1989). Its equation of state included contributions of ideal baryon and photon gases, and of relativistically degenerate electrons. The gravitational potential was computed in monopole approximation, while adding the resulting acceleration in a time symmetric fashion provided second order accuracy.

In order to account for turbulent flame propagation, the program was modified with the SG-model described in Niemeyer & Hillebrandt 1995. All calculations were based on a two-dimensional stationary grid with  $256 \times 64$  zones in spherical  $(r, \vartheta)$  coordinates. Assuming rotational and equatorial symmetry, the boundary conditions were chosen to be reflecting everywhere except at the outer radial edge, where outflow was allowed. Owing to complications with unnaturally high production of SG-turbulence at reflecting walls, both the SG-model and thermonuclear burning were inhibited in close vicinity of the grid boundaries. The zones were placed at equidistant radial and angular intervals with the exception of the 40 outermost ones whose radial separation was defined to increase at a rate of 10 % each. A Cray Y-MP computer at the Rechenzentrum Garching was used for all simulations.

The initial model represented a  $M_{\text{chan}}$  white dwarf with a central density  $\rho_c = 2.8 \times 10^9 \text{ g cm}^{-3}$  and a central temperature  $T_c = 7 \times 10^8 \text{ K}$ . In addition to initial temperature and density profiles a starting value for the turbulent kinetic SG-energy  $q_0$  had to be assigned. Earlier experiments showed that the calcu-

lations are rather insensitive to the choice of  $q_0$  since the SG-model adjusts to the strength of local shear on very short timescales (Niemeyer & Hillebrandt 1995). A reasonable value is provided by the typical convective velocities  $v_{\text{conv}} \approx 5 \times 10^5 \text{ cm/s}$  on the grid scale  $\Delta \approx 10^6 \text{ cm}$  during the pre-ignition phase; this corresponds to  $q_0 \approx 10^{11} \text{ erg/g}$ .

The flame front was initiated by instantly changing the composition of a certain number of zones to nickel while increasing their temperature to several billion degrees, equivalent to raising their internal energy by the binding energy  $\epsilon_{\text{nuc}} \approx 7 \times 10^{17} \text{ erg/g}$ . Immediately after the simulation has started pressure equalizes across the interface of burned and unburned material by emitting weak compression and expansion waves in opposite directions. Meanwhile, turbulent transport increases the temperature in unburned matter surrounding the burned regions and lowers their burning times. After a brief period of burning in the intermediate regime (no flamelets on small scales, transport dominated by turbulence on all scales) a conductive flame front forms after approximately  $10^{-3} \text{ s}$ .

#### 3.1. Centrally ignited deflagrations

In the central ignition (CI) model, a spherical region around the star's center was ignited at  $t = 0 \text{ s}$ . Its surface was perturbed by a periodic pattern with a wavelength of  $\pi/4$  and an amplitude of 25 km; this corresponded to a maximum radial distance of the initial flame front from the star's center of 150 km. The development of the burning front in this and all other models is visualized by snapshots taken at 0.1, 0.8, and 1.4 s. In all figures, the velocity field is represented by randomly selected vector arrows at the respective points, superimposed with contour lines for the density and shaded areas to indicate the energy generation rate.

Shortly after ignition, the flame propagates in a direction normal to its surface and forms a pattern that resembles the cellular structure discussed in Khokhlov 1995 and Niemeyer & Woosley 1996. The cusps pointing toward the burned matter are clearly visible in fig. (2). Large vortices have developed, causing the onset of a turbulent cascade that corresponds to the production of turbulent SG-energy in this model (note that SG-turbulence is only produced in non-burning zones). At  $t \approx 0.1 \text{ s}$ , the turbulent regime dominates over laminar propagation almost everywhere within the front.

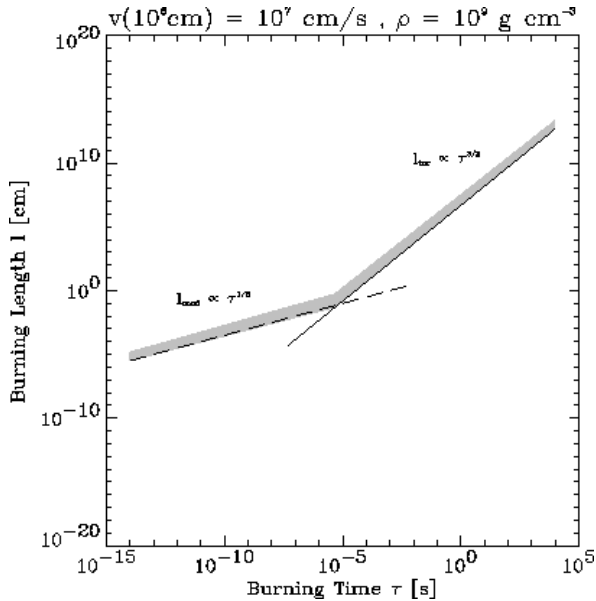


Fig. 1.— Scaling of conductive and turbulent length scales with the burning time. The shaded region marks the dominant burning length scale.

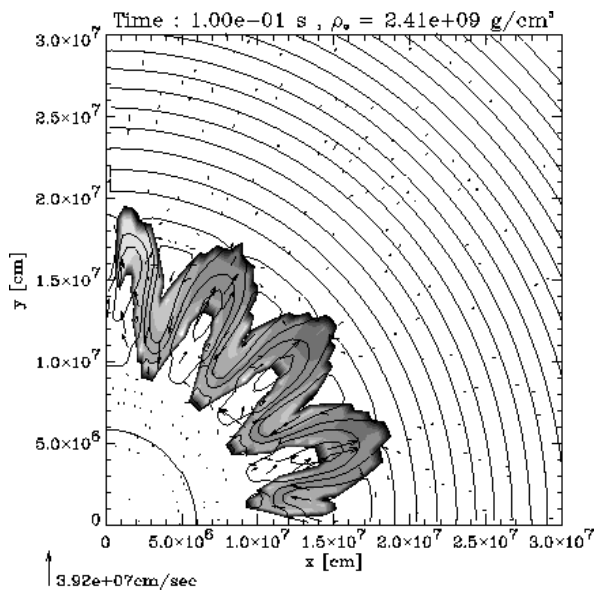


Fig. 2.— Core region in the CI-model shortly after ignition. Density contours are separated by  $\delta\rho = 5 \cdot 10^7 \text{ g cm}^{-3}$ , the maximum energy generation rate (shaded regions) is  $\dot{S}_{\text{max}} = 10^{19} \text{ erg g}^{-1} \text{ s}^{-1}$ .

As the density encountered by the flame brush decreases and effective gravity rises, buoyancy effects begin to govern the front evolution. The cellular structure is disrupted by the formation of hot bubbles floating into the cold material.

At  $t \approx 0.8 \text{ s}$ , displayed in fig. (3), the RT-instability of the burning front has developed to its maximum extent. The turbulent flame speed is now  $u(\Delta) \approx 2 \times 10^7 \text{ cm/s}$  at the points of maximum turbulent subgrid energy. Four major bubbles can be identified, separated by thin streams of unburned C+O-material. As Khokhlov 1994 points out, this particular pattern is an artifact of the two-dimensional simulation, as opposed to an increased fragmentation of the front in three-dimensional calculations. Since the material velocity on large scales is governed by buoyancy and the small scales behave as if fragmented in three-dimensional turbulence by virtue of the SG-model, the consequences of this effect may not be essential. However, as more efficient fragmentation also leads to an increased production of turbulence it is possible that it indirectly alters the strength of the explosion. It is still necessary to confirm this assertion by means of three-dimensional simulations.

After the star has expanded and the density of the burning region has fallen to some  $10^7 \text{ g cm}^{-3}$ , the flame is extinguished at low densities. In our code, this occurs when  $l_{\text{burn}} \approx \Delta$ . At this stage, incomplete nuclear burning presumably produces intermediate mass elements that can be observed in SN Ia spectra. The simple network employed in this work is unable to predict the final composition of the burning products at densities below  $10^7 \text{ g cm}^{-3}$ . Therefore, the exact results of this stage of our simulations have to be interpreted with some care, since they can only qualitatively represent the physically realistic behavior of a dying flame. However, the energetical aspects of the explosion are widely unaffected by this shortcoming and may therefore be taken at face value. It is also possible to give an estimate of the amount of intermediate mass elements produced in our models by keeping track of the amount of burned matter as a function of burning density (see section 4).

### 3.2. Off-center ignition at one point

GW's arguments suggest that flame ignition may occur on the surface of buoyant bubbles that have already risen to radial distances of approximately 200 km. According to their estimates, the bubbles have diameters of some 10 km and velocities around 100

km/s at the time of flame formation. In order to study the effects of off-center ignition we carried out a number of simulations where the flame was ignited at only one point located at a radius of 200 km. As only one zone was initially burned in these one bubble (1B)-models, the radius of the ignited region roughly equaled  $0.5\Delta \approx 5$  km. Some trial calculations involved giving the ignited zone an initial velocity of 100 km/s, but after very short times the velocity field relaxed to the same solution as in the case of an initially resting ignition zone. It should be kept in mind in the ensuing discussion that the assumption of rotational and equatorial symmetry enters strongly in this simulation. Despite the fact that the actual structure of the burning front represents two toroidal buoyant rings we shall keep the term “bubble” in the following description of the front evolution.

The bubble quickly attains a drop-like shape and instantly begins to float with some  $10^7$  cm/s (fig. 4). The energy generation rate is weak compared with the CI-model at the same time, resulting from the lack of strong shear flows. This can be explained by the larger amount of potential energy of hot material in the CI-model at the time of ignition. It is quickly transformed into kinetic energy as the RT-structures begin to float, giving rise to the production of turbulent SG-energy. The floating volume in the 1B-model, on the other hand, is smaller in the beginning and therefore unable to provide a large amount of turbulent kinetic energy to accelerate the burning front.

Having reached a maximum radial extent of approximately 450 km and a rising velocity of more than  $10^8$  cm/s, the bubble begins to spread out in the angular dimension. fig. (5) shows the burning bubble in the fully developed “mushroom stage”: a nearly spherical head with a diameter of roughly 500 km is attached to a thin pole that connects it to the center of the expanding star. The most prominent feature of this configuration is the large volume of burning material at low densities compared to the part of the front that burns at higher density. It may help to account for the production of intermediate mass elements necessary to reproduce SN Ia spectra. A more detailed discussion of this aspect will follow in section (4).

### 3.3. Ignition at five points

As only little is known about the circumstances of flame ignition it is also possible that ignition occurs at many points scattered throughout the white dwarf

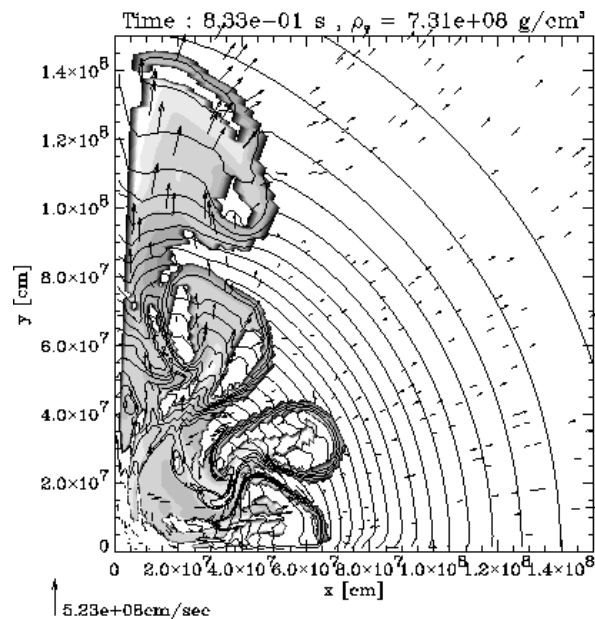


Fig. 3.—  $\delta\rho = 3 \cdot 10^7$  g cm $^{-3}$ ,  $\dot{S}_{\max} = 1.3 \cdot 10^{19}$  erg g $^{-1}$  s $^{-1}$ .

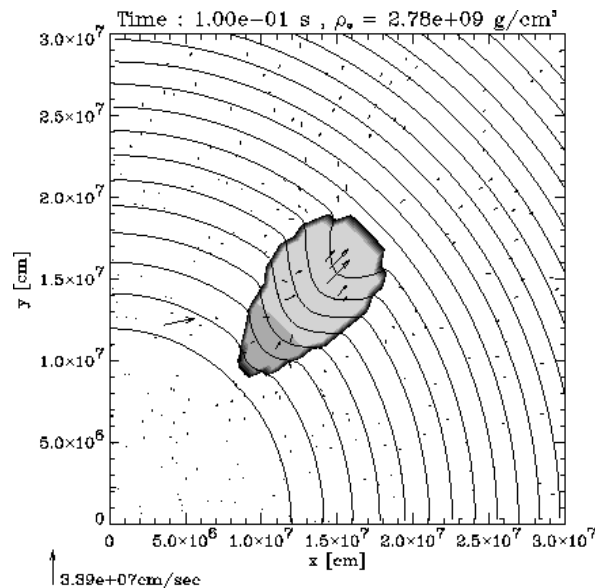


Fig. 4.— 1B-model with  $\delta\rho = 6 \cdot 10^7$  g cm $^{-3}$  and  $\dot{S}_{\max} = 7 \cdot 10^{18}$  erg g $^{-1}$  s $^{-1}$ .

core region almost simultaneously. The multiple ignition model (specifically, ignition at five points (5B)) can be viewed as a compromise between the instantaneous incineration of the core region at  $t = 0$  and ignition at only one point. This way, some desirable properties of both the CI-model (strong velocity gradients triggering a powerful turbulent cascade) and the 1B-model (burning at lower density, increasing the synthesis of intermediate mass elements) may be combined.

The model presented here differs from the standard models described for the CI and 1B-cases with respect to the turbulent diffusion coefficient  $C_{\epsilon_1}$  (section 2). While  $C_{\epsilon_1} = 2$  was used in all other simulations of turbulence dominated flames this calculation was carried out with  $C_{\epsilon_1} = 1$ . It therefore models a slightly more slowly propagating flame front, while the burning rate remained unchanged. In order to assess the influence of the propagation and burning rates on the explosion a second simulation with identical initial conditions but different calibration parameters ( $C_{\epsilon_1} = 2$  and  $\mathcal{B} = 0.511$ ) was carried out; in section (4), these models are referred to as the “slow” and “fast” 5B-models, respectively.

The initial ignition pattern chosen for the 5B-model can be seen in fig. (6). Three zones were incinerated at  $r \approx 100$  km while two more bubbles were triggered at  $r \approx 200$  km. This choice follows from the intuitive notion that ignition is more likely at higher temperatures closer to the center. Initially, all five bubbles evolve independently, floating in the same way as described for the 1B-model. After a short time, the bubbles begin to interact. As a consequence of their lower buoyant speed the inner three bubbles merge first, later joined by the upper two.

It is interesting to compare fig. (7) with figs. (3) and (5). While the maximum material velocity (shown at the bottom of the plots) of the 5B-model equals that of the central ignition calculation, its central density is considerably lower. Furthermore, most of the burning material is further off center and therefore burns at a lower average density, similar to the 1B-model. However, the energy generation rate in the 5B-model is higher than in the latter, indicating stronger turbulent motions. The apparent similarity of front evolution in both off-center models and their difference from the CI-simulation gives evidence that under most natural initial conditions, the bulk volume of burning material can be expected to float upward. The fact that this is not observed in central

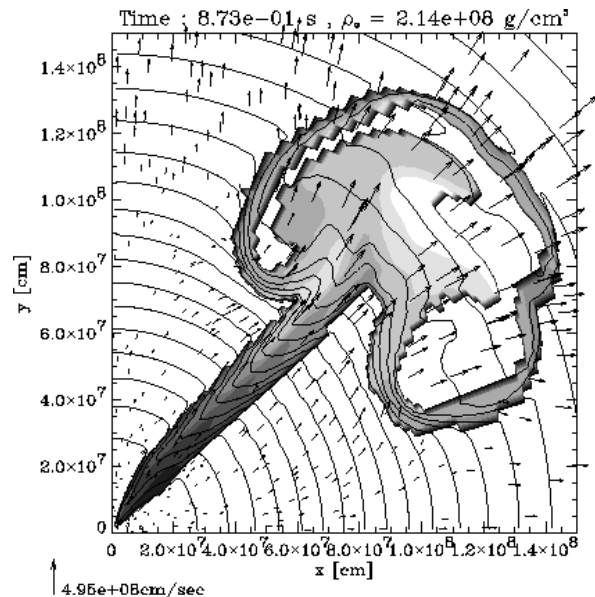


Fig. 5.—  $\delta\rho = 10^7$  g cm $^{-3}$ ,  $\dot{S}_{\max} = 10^{19}$  erg g $^{-1}$  s $^{-1}$ .

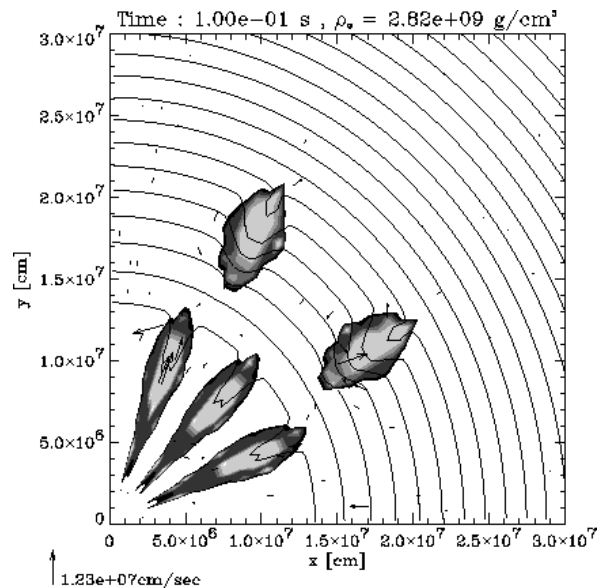


Fig. 6.— “Slow” 5B-model;  $\delta\rho = 6 \cdot 10^7$  g cm $^{-3}$  and  $\dot{S}_{\max} = 6 \cdot 10^{18}$  erg g $^{-1}$  s $^{-1}$ .



ignition simulations is probably related to the symmetry conditions that are usually imposed at the grid boundaries.

At the time of flame extinction, the high extent of fragmentation compared with the other models becomes visible. The flame covers a substantial part of the picture and still burns strongly in regions of higher density. This fact explains the higher release of energy in the 5B-explosion compared with the other models (section 4).

#### 4. Global energetic parameters

The most important parameter to determine the final fate of the white dwarf is its total energy. So far, all multidimensional simulations of the problem have failed to release the required  $\gtrsim 0.5 M_{\odot}$  in the first deflagration phase needed to account for SN Ia observations, therefore implying pulsational detonations if Chandrasekhar mass models were to explain these events (Khokhlov 1995, Arnett & Livne 1994a, Arnett & Livne 1994b). The simulations presented in this work provide a possible explosion mechanism without involving detonations, but the explosions are still too weak to explain most Type Ia supernovae. This can be seen in fig. (8), showing the total energy as a function of time. All models start at a value of approximately  $-5 \times 10^{50}$  erg, consisting mostly of negative gravitational energy and positive Fermi energy of the degenerate electron gas. Note that the CI-model (solid line) has a slightly higher total energy at  $t = 0$  which is related to the larger initially incinerated mass.

The only model that remains bound after burning has ceased is the 1B-simulation. It burns less than  $0.3 M_{\odot}$  in the first deflagration phase and is thus the only candidate for a pulsational detonation. According to the description in section (3.2), the front fails to ignite a sufficiently large volume because of its limited volume and the lack of fragmentation. While the latter aspect may change in a three dimensional treatment, it must be stressed that the simulation already assumes rotational and equatorial symmetry. Three-dimensional simulations of the full star would therefore show a much smaller volume of the burning bubble and thus predict the generation of considerably less energy. Hence, it is unlikely that one-point ignitions yield enough energy for a healthy explosion on the first try unless the burning front spreads significantly faster than modeled.

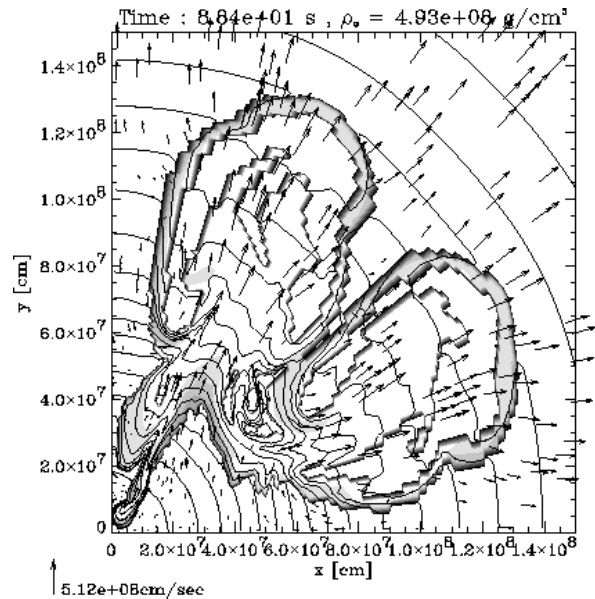


Fig. 7.—  $\delta\rho = 3 \cdot 10^7 \text{ g cm}^{-3}$ ,  $\dot{S}_{\text{max}} = 10^{19} \text{ erg g}^{-1} \text{ s}^{-1}$ .

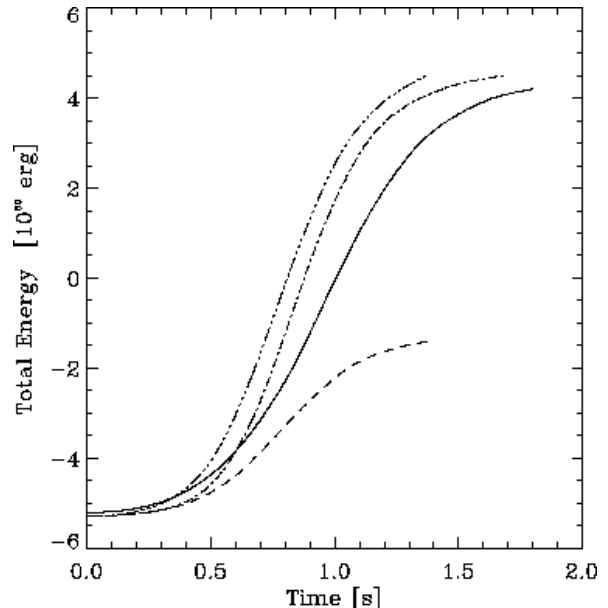


Fig. 8.— Total energy of the different models as a function of time (— CI, -- 1B, - - - slow 5B, - · · · fast 5B).

One may, of course, speculate about the subsequent evolution of the 1B-model. Some burning material, surrounded by large amounts of unburned carbon and oxygen, probably remains in the flamelet regime until the star recontracts. Re-ignition could then occur on a highly convoluted and aspherical surface that results from folding and compression of the thin stream of burning matter reaching toward the center. Whether this process is able to form a detonation, or else produces more buoyant bubbles with turbulent burning surfaces cannot be answered at this point. In order to obtain information about the re-ignition phase the multidimensional evolution has to be followed for several seconds after the initial deflagration, which is computationally unfeasible at present.

The CI-explosion terminates burning after producing  $0.59 M_{\odot}$  of nuclear fuel, which represents the energetical threshold of an observable, but weak, SN Ia event. Despite its higher mass of initially burned material and the relatively large surface of the burning front it releases less energy than the 5B-models.

Finally, both fast and slow 5B-simulations appear to represent possible candidates for some Type Ia supernovae. Independent of the variations in burning and propagation speed mentioned in section (3.3), between  $0.65 M_{\odot}$  and  $0.67 M_{\odot}$  matter are burned, liberating approximately  $9 \times 10^{50}$  erg of nuclear energy (this number is slightly overestimated due to our assumption of NSE even at low burning densities, see the next paragraph).

To conclude the discussion of the performed numerical experiments some implications for nucleosynthesis in SN Ia events shall be pointed out. On account of the simplified nuclear network that implies NSE for the burning products, only indirect statements about the expected final composition are possible. For this reason, the amount of burned carbon and oxygen as a function of burning density is plotted in fig. (9) for all models. Of particular interest is the region below  $10^7 \text{ g cm}^{-3}$  where intermediate mass elements begin to be synthesized. The solid curve, representing the CI-model, shows a sharp peak at approximately  $4 \times 10^8 \text{ g cm}^{-3}$  followed by a rapid decline toward lower densities. Very little burning occurs in the intermediate mass region. On the other hand, all three off-center simulations burn significantly larger amounts of matter below  $10^7 \text{ g cm}^{-3}$ . Most surprising is the ratio of this value to the total amount of burned matter for the 1B-model: it reaches 20 percent, compared to only four percent for the CI-model. Addi-

tional information about the expected nucleosynthesis can be gained from the region above  $\approx 1.5 \times 10^9 \text{ g cm}^{-3}$ . There, the high electron density leads to excess neutronization compared to solar composition (Woosley 1990). As expected, the 1B-model burns the smallest amount of C+O-matter at high densities. However, both 5B-models burn even more than the CI-simulation which might be explained by the rapid initial expansion of the latter during the first  $10^{-2}$  s because of its higher mass of initially ignited material.

The total mass of burned material near the end of the simulations is summarized in table (1), together with the parameters of equations (7) and (10) used for the different models.

## 5. Conclusions

It can reasonably be assumed that flame ignition in  $M_{\text{chan}}$  models for white dwarf explosions occurs under convective conditions that make ignition at the precise center unlikely. Based upon a simple model for the ignition process (GW), we expect that *in general*, ignition will occur at one or many points within the core. Three models were studied in two-dimensional simulations: ignition at one (1B) and five (5B) points slightly off-center, in addition to the standard central ignition (CI) scenario.

The overall appearance of both off-center models is strikingly different from the CI-case. As the bubble (or its merging components) rises, it leaves behind a trail of burning material while the uppermost part grows rapidly. At the maximum of global energy generation the shape of the burning front resembles a mushroom whose wide head is supported by a thin pole that reaches from the center to about a third of the star's radius. Various processes are responsible for this structure: first, the turbulent flame speed is much less at the bottom because of the smaller velocity gradients and shear stress. Therefore, angular spreading at the pole happens at a smaller rate than in the stirred upper region. Equally important is the flow pattern around and within the bubble: displacement of cold material by the rising volume creates large vortices that diverge at the top and converge at the bottom of the bubble, thereby focusing the pole and expanding the top. They also cause the high burning velocities in the upper part by creating high velocity gradients in the mixing region. Formation of the macroscopic vortices therefore also determines

the radius (and, consequently, density) at which the bubble begins to spread out. In the simulations, this happens at approximately one third to one half of the star’s radius. It must be kept in mind that the details of this development, in particular the formation of large scale vortices, are probably different in three-dimensional reality.

The RT-fingers of the CI-model display similar characteristics on smaller scales, but never develop the same elongated mushroom shape. This is at least partly due to the fact that initial perturbations first have to overcome the linear RT growth stage before becoming fully buoyant. By the time the nonlinear evolution sets in, the dynamics of the largest scales is already strongly influenced by the expansion of the star. From this point of view, off-center ignition models simply skip the linear instability regime and consequently gain important time to rise and become turbulent. The most important consequence of this behavior is a higher total burning rate at early times than predicted by standard deflagration scenarios. We can expect this effect to be even more pronounced in three dimensions and with a large number of initial ignition points. If ignition occurred almost simultaneously throughout the central region, but located on bubble surfaces with small radii compared to that of the ignition region, the bubbles would reach their maximum burning rate at roughly the same time. The amount of matter that has been burned by then, which in turn determines the degree of expansion of the star at the time rapid burning sets in, will have to be calculated by three-dimensional simulations with high resolution.

A rough estimate of the average bubble velocity in the limit of many interacting bubbles in three dimensions can be obtained from experiments (Read 1984, Snider & Andrews 1994) and simulations (Youngs 1984, Li 1996) of RT mixing fronts in the fully nonlinear regime. It was shown that the front boundary propagates into the unmixed fluid with the velocity

$$v_{\text{front}} = 2 \alpha g_{\text{eff}} t , \quad (11)$$

independent of the initial conditions. Here,  $t$  is the time since the beginning of the nonlinear RT stage and  $\alpha \approx 0.07$  is a constant. This behavior was successfully explained by statistical models pioneered by Sharp and Wheeler (Sharp 1984) and refined by Glimm & Li 1988, Glimm & Sharp 1990 and Zhang 1990. The Sharp-Wheeler model assumes that interacting bubbles merge to form bigger ones while small

bubbles are being washed downstream, thus increasing the average bubble radius  $\langle r \rangle$  at the front boundary. Together with the rise velocity of single bubbles (7), this process can account for a constant increase of  $v_{\text{front}}$ . It is easily seen that (7) and (11) agree if  $\langle r \rangle$  grows linearly with the distance of the bubbles from the inner front boundary, which is in our case equal to the size of the burned out region (this is also clear from dimensional analysis). Furthermore, our bubbles increase their volume by rapid burning and by gas expansion, providing additional growth as they rise outward. Hence, equation (11) is a reasonable approximation even if bubble merging is not the dominant dynamical effect. Using typical numbers for white dwarf explosions,  $g_{\text{eff}} \approx 10^9 \text{ cm s}^{-2}$  and  $t \approx 1 \dots 2 \text{ s}$ , we obtain front velocities of the order of  $2 \times 10^8 \text{ cm s}^{-1}$ . According to one dimensional studies (Woosley 1990) with similar velocities, this front velocity is sufficient to produce a healthy explosion.

As a second result of off-center ignition, considerably more matter is burned in a lower density environment than in the central ignition simulation (table 1). This helps to satisfy two major constraints on potential SN Ia explosion mechanisms: only little nuclear burning at high density is permitted to limit the overproduction of neutron-rich isotopes, and a large amount of intermediate mass nuclei produced at  $\rho \lesssim 10^7 \text{ g cm}^{-3}$  is required to explain the observed spectral lines (Woosley 1990). Comparing the respective ratios of both masses and the total burned matter, the 1B-model is clearly the best candidate in this particular respect. While the 5B-models produce large amounts of intermediate mass isotopes they also burn more high density material than the CI-model. In the overall comparison of the expected nucleosynthesis, however, all off-center models are closer to the expectations from SN Ia observations and solar abundance studies (Woosley 1990) than the CI-model.

Looking at the final values for the total energy the 1B-model fails to be a Type Ia supernova (neglecting the possibility of a pulsational detonation). Despite the symmetry assumptions that imply identical energy generation in both hemispheres, too little nuclear energy is released to unbind the star. We can therefore conclude that in order to produce a successful explosion in the first deflagration phase, flame ignition must occur at a number of points within a short period of time (less than  $\approx 10^{-1} \text{ s}$  when the star begins to expand), where the term “points” refers to regions with a diameter equal to or less than 10 km (the

size of our grid zones). Both 5B-simulations and the CI-model become unbound during their explosions. However, the CI-case would only represent a weak SN Ia since it barely produces the minimum value of approximately  $0.6 M_{\odot}$  (table 1) of nuclear burning products necessary to account for light curves and kinetic energy of the ejecta (e.g., Woosley 1990). The 5B-calculations, on the other hand, are in most respects possible candidates for some SN Ia events, although the final amount of produced  $^{56}\text{Ni}$  is still insufficient to account for the light curves of the full class of explosions. We can thus summarize that deflagration models of  $M_{\text{chan}}$  white dwarfs with a small number of burning bubbles are unlikely to produce powerful SN Ia's unless our simulations fail to cover the relevant physics. In addition to the expected changes in three dimensions described above, examples for potentially important, but neglected effects include the additional production of turbulence by burning itself (Niemeyer & Woosley 1996) or from differential rotation of the star.

Of course, all results of supernova simulations have to be placed in the context of their numerical technique. In our case, two numerical tools, the SG model for unresolved turbulence and the flame propagation algorithm, deserve closer inspection as they are both new and crucial ingredients in our work. The SG model and some of its numerical properties have been discussed in (Niemeyer & Hillebrandt 1995 and references therein). Within its limits (no production of turbulence by thermal expansion within the flame brush, artificial closure assumptions) it is capable of representing the unresolved turbulence in a way that we consider realistic. Dramatic changes in the outcome of the simulations by changing the SG parameters within reasonable limits cannot be expected (Niemeyer & Hillebrandt 1995). The same is true for the flame algorithm, whose performance has been tested in Niemeyer 1995. However, more effort is necessary to study the problem of numerically representing turbulent flame fronts in finite difference schemes like PPM. So far, the turbulent flame brush has either been treated like a thin, laminar flame surface that moves with the turbulent burning speed (Khokhlov 1995, Niemeyer & Hillebrandt 1995), or has been smeared out over a large region by turbulent diffusion (this work). Both methods are probably wrong, at least to some extent. It cannot be excluded that increasing the numerical resolution and our ability to model turbulent flames will change our results,

although it is unclear in which direction.

The possible transition to a delayed or, in case of the 1B model, pulsational detonation has not been considered in this work but remains, in principle, a viable option for SN Ia models. However, all of our results show subsonic effective burning velocities at all times during the turbulent deflagration phase, making the delayed formation of a detonation very unlikely. Again, the situation may turn out differently if one considers an ensemble of many bubbles that start interacting almost simultaneously.

The sensitivity of our results to the initial conditions opens a new dimension of parameter space that is worth exploring. One can speculate that some of the variations noticed in SN Ia observations can be accounted for by this effect. However, if ignition occurs at sufficiently many points throughout the core region, the outcome is again expected to be statistically homogeneous. Detailed studies of the ignition process will be necessary to answer this question.

We would like to express our thanks to S. Blinnikov and A. Kerstein for interesting discussions on flame physics, and to E. Müller for assistance with the numerical experiments. We also thank the referee F.X. Timmes for helpful suggestions to improve this manuscript. JCN and WH acknowledge the hospitality of UCO/Lick Observatories where some of this work was carried out. JCN was supported by a DAAD HSP II/AUFE fellowship. SEW was supported by the NSF (AST 9115367; AST 94-17161), NASA (NAGW 2525; NAG5-2843), and, in Munich, by an award from the Humboldt Foundation.

TABLE 1  
 SUBGRID PARAMETERS AND BURNED MASSES AFTER  $t \approx 1.4$  s FOR ALL MODELS.

Model	$\mathcal{B}$	$C_{\epsilon_1}$	$M_b [M_\odot]$	$M_b(\rho \gtrsim 1.5 \cdot 10^9) [M_\odot]$	$M_b(\rho \lesssim 10^7) [M_\odot]$
CI	0.25	2	0.59	$3.5 \cdot 10^{-2}$	$2.5 \cdot 10^{-2}$
1B	0.25	2	0.27	$1.1 \cdot 10^{-2}$	$5.3 \cdot 10^{-2}$
5B, slow	0.25	1	0.65	$4.5 \cdot 10^{-2}$	$6.9 \cdot 10^{-2}$
5B, fast	0.511	2	0.67	$4.8 \cdot 10^{-2}$	$8.3 \cdot 10^{-2}$

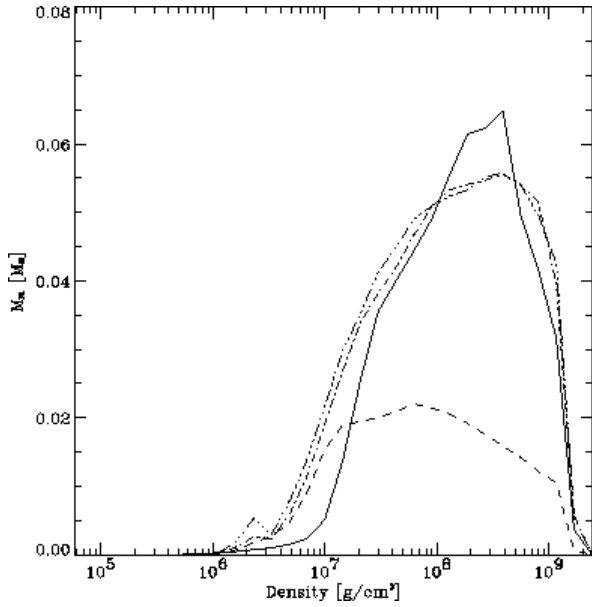


Fig. 9.— Mass of burned matter as a function of the burning density at  $t \approx 1.4$  s (— CI, -- 1B, - · - slow 5B, · · · fast 5B).

## REFERENCES

- Arnett, W. D., & Livne, E. 1994a, *ApJ*, 427, 315
- Arnett, W. D., & Livne, E. 1994a, *ApJ*, 427, 330
- Benz, W. 1996, in *Thermonuclear Supernovae*, eds. R. Canal & P. Ruiz LaPuente, in press.
- Fryxell, B.A., Müller, E., & Arnett, W.D. 1989, *MPA Preprint Series*, 449
- Garcia-Senz, D., Bravo, E., & Woosley, S. E. 1996, in *Thermonuclear Supernovae*, eds. R. Canal and P. Ruiz-LaPuente, in press
- Garcia-Senz, D., & Woosley, S. E. 1995 (GW), *ApJ*, 454, 895
- Glimm, J., & Li, X.L. 1988, *Phys. Fluids*, 31, 2077
- Glimm, J., & Sharp, D.H. 1990, *Phys. Rev. Lett.*, 64, 2137
- Höflich, P., & Khokhlov, A. 1996, *ApJ*, in press.
- Iben, I., Jr. 1982, *ApJ*, 253, 248
- Iben, I., Jr., & Tutukov, A. V. 1991, *ApJ*, 370, 615.
- Kenyon, S. J., Livio, M., Mikolajewska, J., & Tout, C. A. 1993, *ApJ*, 407, L81
- Khokhlov, A.M. 1991a, *A&A*, 245, 114
- Khokhlov, A.M. 1991b, *A&A*, 245, L25
- Khokhlov, A.M. 1991c, *A&A*, 246, 383
- Khokhlov, A.M. 1993, *ApJ*, 419, L77
- Khokhlov, A.M. 1994, *ApJ*, 424, L115
- Khokhlov, A.M. 1995, *ApJ*, 449, 695
- Landau, L.D., & Lifshitz, E.M. 1991, *Lehrbuch der Theoretischen Physik VI: Hydrodynamik* (Berlin: Akademie-Verlag)
- Layzer, D. 1955, *ApJ*, 122, 1
- Li, X.L. 1996, *Phys. Fluids*, 8, 336
- Limongi, M., & Tornambe, A. 1991, *ApJ*, 371, 317.
- Livne, E. 1993, *ApJ*, 406, L17
- Livne, E., & Arnett, W.D. 1996, in *Thermonuclear Supernovae*, eds. R. Canal & P. Ruiz LaPuente, in press
- Müller, E. 1994, *Fundamentals of Gasdynamical Simulations*, *MPA Preprint Series*, 780
- Müller, E., & Arnett, W.D. 1986, *ApJ*, 307, 619
- Munari, U., & Renzini, A. 1992, *ApJ*, 397, L87
- Niemeyer, J.C. 1995, Ph.D. Thesis, *MPA Preprint Series*, 911
- Niemeyer, J.C., & Hillebrandt, W. 1995, *ApJ*, 452, 769
- Niemeyer, J.C., & Woosley, S.E. 1996, *subm. to ApJ*
- Nomoto, K., Thielemann, F.-K., & Yokoi, K. 1984, *ApJ*, 286, 644
- Rappaport, S., Di Stefano, R., & Smith, J. D. 1994, *ApJ*, 426, 692
- Read, K.I. 1984, *Physica D*, 12, 45
- Sharp, D.H. 1984, *Physica D*, 12, 3
- Snider, D.M., & Andrews, M.J. 1994, *Phys. Fluids*, 6, 3324
- Timmes, F.X., & Woosley, S.E. 1992, *ApJ*, 396, 649
- Woosley, S.E. 1990, in *Supernovae*, ed. A.G. Petschek (Berlin: Springer-Verlag), p.182
- Woosley, S. E., and Eastman, R. G. 1995, *Proceedings of Menorca School of Astrophysics*, eds. E. Bravo, R. Canal, J. Ibanez, and J. Isern, *Societat Catalana de Fisica*, p. 105
- Woosley, S. E., & Weaver, T. A. 1986, in *Radiation Hydrodynamics in Stars and Compact Objects*, eds. D. Mihalas & K.-H. A. Winkler, (Springer Verlag:Berlin), p. 91
- Woosley, S. E., & Weaver, T. A. 1994a, *ApJ*, 423, 371.
- Youngs, D.L. 1984, *Physica D*, 12, 32
- Zhang, Q. 1990, *Phys. Lett. A*, 151, 18